Diet Induced Obesity and Diabetes Enhance Mortality and Reduces Vaccine Efficacy for SARS-CoV-2

Robert M Johnson[1], Jeremy Ardanuy[1], Holly Hammond[1], James Logue[1], Lian Jackson[1], Lauren Baracco[1], Marisa McGrath[1], Carly Dillen[1], Nita Patel[2], Gale Smith[2], Matthew Frieman[1]

1. Center for Pathogen Research, Department of Microbiology and Immunology, University of Maryland School of Medicine, Baltimore, MD, 20201
2. Novavax, Gaithersburg, MD.

Abstract

Severe Acute Respiratory Syndrome Coronavirus-2 (SARS-CoV-2), the causative agent of Coronavirus disease 2019 (COVID-19), emerged in Wuhan, China, in December 2019. As of October 2022, there have been over 625 million confirmed cases of COVID-19, including over 6.5 million deaths. Epidemiological studies have indicated that comorbidities of obesity and diabetes mellitus are associated with increased morbidity and mortality following SARS-CoV-2 infection. We determined how the comorbidities of obesity and diabetes affect morbidity and mortality following SARS-CoV-2 infection in unvaccinated and adjuvanted spike nanoparticle (NVX-CoV2373) vaccinated mice. We find that obese/diabetic mice infected with SARS-CoV-2 have increased morbidity and mortality compared to age matched normal mice. Mice fed a high-fat diet (HFD) then vaccinated with NVX-CoV2373 produce equivalent neutralizing antibody titers to those fed a normal diet (ND). However, the HFD mice have reduced viral clearance early in infection. Analysis of the inflammatory immune response in HFD mice demonstrates a recruitment of neutrophils that was correlated with increased mortality and reduced clearance of the virus. This model recapitulates the increased disease severity associated with obesity and diabetes in humans with COVID-19 and is an important comorbidity to study with increasing obesity and diabetes across the world.

Corresponding author:
Matthew Frieman, PhD., Department of Microbiology and Immunology, University of Maryland School of Medicine, Baltimore, MD. mfrieman@som.umaryland.edu

Introduction

The United States of America has an obesity rate of 42%, diabetes rate of 11%, and 35 % of the population has been identified as prediabetic[1]. Epidemiologic studies of COVID-19 have identified obesity and diabetes as significant risk factors for increased disease severity, length of hospitalization, and death[2-5]. The immune and molecular mechanisms behind this increased risk of COVID-19 have yet to be fully determined. SARS-CoV-2 is not the only coronavirus linked to increased disease severity in those with diabetes or obesity. The Middle East respiratory syndrome coronavirus (MERS-CoV), first identified in 2012, was clinically and experimentally linked to increased diease severity in those with diabetes[6, 7], with diabetics have a 7-fold higher odds ratio of severe disease and death after MERS-CoV infection. MERS-CoV also demonstrated increased morbidity and mortality in an obese/diabetic mouse models , with HFD mice presenting with increased lung pathology, viral titer and a dysregulated immune response MERS-CoV infection [7-9].

To study the role of obesity and diabetes in SARS-CoV-2, we utilized a mouse model where mice are fed a high fat diet (HFD) (60% fat) starting at 3 weeks of age. By 14 weeks of age, HFD mice are obese, glucose intolerant and have high resting glucose levels; all metrics of having Type 2 diabetes (T2D). Infection of ND and HFD mice with SARS-CoV-2 (MA10 mouse adapted strain) demonstrates lethal disease in HFD only mice by 7 dpi. Equivalent viral lung titers were found in both ND and HFD mice, but increased lung inflammation was observed in HFD (obese/diabetic) mice. Vaccination of ND and HFD mice with the saponin-based Matrix-M adjuvanted spike nanoparticle (NVX-CoV2373)[10, 11] resulted in generation of similar levels of neutralizing antibody. However, when challenged with SARS-CoV-2 (MA10), HFD mice had a delay in clearance with little reduction in lung titer. Evaluation of the inflammatory response in HFD vaccinated/infected mice found an increase in neutrophils in lung infiltrate that correlated with an increased innate inflammatory response. We believe this demonstrates a dysregulated immune response in obese/diabetic mice leading to increased morbidity and mortality as well as potentially skewing the quality of protection from vaccination. This supports what is seen in diabetic and obese humans throughout the COVID-19 pandemic and provides a model to identify the molecular and immunological mechanisms underlying the response to SARS-CoV-2 in this population.

Results

High fat diet fed mice have obesity and type 2 diabetes

To study the effects of obesity and diabetes on SARS-CoV-2 infection, we established a model of SARS-CoV-2 infection based on the previously established HFD fed model. At the time of weaning (~3

weeks), C57/B6 mice are placed on a ND (18% kcal from fat, 24% kcal from protein, and 58% kcal from carbohydrates) or a HFD (60% kcal from fat, 18% kcal from protein, and 21% from carbohydrates). At 18 weeks of age, 15 weeks on each diet, we analyzed fasting blood glucose (Figure 1B), fasting serum insulin (Figure 1C), HOMO-IR (Figure 1D) and weight (Figure 1E). The HFD mice had increased fasting blood glucose, fasting serum insulin, HOMO-IR and higher weight, which are all parameters of obesity, insulin resistance and T2D. Once established, 18 week old ND and HFD mice were then used for pathogenesis and vaccination experiments throughout the study.

SARS-CoV-2 infected obese/diabetic mice have increased morbidity and mortality

ND and HFD mice were infected with the SARS-CoV-2 (MA10)[12] strain at 10^3 and 10^5 PFU per mouse. Mice were weighed daily for 7 days, with lungs evaluated on 2, 4 and 7 days post-infection (dpi). ~20% of the ND mice infected with 10^3 or 10^5 PFU MA10 died by 7 dpi (Figure 1A). However, for HFD mice infected with 10^3 PFU and ~40% die by day 7. Most notably, 100% death was observed in the 10^5 PFU infected HFD group. The kinetics of lethality varied between groups as well, with 20% of the HFD mice dying by day 3 whereas the ND mice did not die until at least 5 dpi.

Weight loss was followed through 7 dpi in all groups (Figure 2). For the low infection dose, we observed the ND mice starting to lose weight at 2 dpi with a total weight loss of around 20% by at 7 dpi. The HFD mice lost weight starting 2 dpi, but it only continued until 4dpi, for a total loss of around 10% and was maintained for the remainder of the experiment. For the high infection dose, the ND mice lost weight starting on 2 dpi and continued through the day 7 endpoint of this experiment with a total weight loss of thirty percent (Figure 2C). The HFD mice lost weight starting on 2 dpi and continued until succumbing to the infection on 5 dpi (Figure 2C). As ND mice weigh less than HFD mice, analysis of by grams of weight lost intra group, as compared to total %, can provide additional insight. Here, when we compare the ND and NFD mice, no differences were observed (Figure 2D & E).

We next examined viral replication in the lungs of infected mice at 2, 4, and 7 dpi. For all groups, the peak viral replication occurred at 2 dpi with a viral titer ~10^8 pfu/g of lung and decreased through day 7 (Figure 2F). At 4 dpi, we observed less viral titer in the 10^5 PFU group compared to the 10^3 PFU group (Figure 2F). This was surprising; however, we suspect that the reduced viral titer in the high dose lungs is potentially due to either reduced numbers of infectable cells at this timepoint due to virus induced cell death or a large influx of inflammatory cells, potentially limiting replication but not enough to protect from death.

Obese/diabetic mice have no difference in lung pathology after infection with SARS-CoV-2

At the low infectious dose, both HFD and ND mice show similar lung pathology that is characterized by a mixed inflammatory infiltrate that peaks at 4 dpi and begins to resolve by 7 dpi. Epithelial cell sloughing in the bronchi is observed starting at 2 dpi with epithelial cells replaced by 7 dpi in most large airways. An observable level of edema is also visible in both HFD and ND lungs across time points (Figure 3A).

At the high infectious dose, the course of inflammation in the lung is similar but more severe than at the low dose. Mixed inflammatory infiltrates in the alveolar space are observed beginning at 2 dpi and increasing through 7 dpi for the surviving ND mice. The infiltrates are predominantly comprised of neutrophils and monocytes, as observed by H&E and quantified by flow cytometry analysis (Figure 7). Bronchiolar sloughing is also more pronounced at the high infectious dose, with visible damage still present at 7 dpi. Perivascular cuffing and edema were also observed in the high infectious dose mice (Figure 3A).

Lung sections were stained for the presence of nucleocapsid (N) protein using immunohistochemistry as a way to visualize the antigen localization within the lung sections and to determine if HFD caused broader spread of infection than ND fed mice. Similar to what was observed by viral titer, the amount of N staining is highest at 2 dpi, with the majority of N localizing in the ciliated epithelial cells of the large airways for both the control and HFD mice (Figure 3B). We detect a small amount of N positivity outside the airways, most noticeably at 4 dpi (Figure 3B). Sections from 7 dpi show little to no N staining positivity, correlating with the viral clearance pattern observed by the viral titer (Figure 3B). No differences are observed between ND and HFD mice demonstrating that HFD mice have no changed in virus tropism. Taken together this data demonstrates that obesity/diabetes increases the mortality of a SARS-CoV-2 infection. This increased mortality is not due to an increase in weight loss, viral titer, lung pathology or viral dissemination.

Obese/diabetic mice have altered host immune responses after infection with SARS-CoV-2

As obesity/diabetes is known to augment the host immune response[13-17], we examined the cytokine and chemokine profile of uninfected, SARS-CoV-2 infected ND and HFD mice. To perform a longitudinal analysis, we used the $1x10^3$ pfu/ mouse dose to allow for a time course across 7 dpi. Via transcriptional analysis of lung tissue, we investigated the changes in expression for a variety of chemokine and cytokine genes in both ND and HFD mice. On days 2 and 4 post-infection, we observed an overall upregulation of cytokines, chemokines, and growth factors associated with neutrophil

recruitment and activation in HFD compared with ND mice (Figure 4). In contrast, by 7 dpi, we observe down-regulation of many of the same pro-inflammatory genes (Figure 4). Interestingly, we observe that HFD mice had a ~3 fold down-regulation of IL1-β, which is a mediator of lung inflammation, fever and fibrosis (Figure 4).

Vaccinated HFD mice suffer from weight loss and have delayed clearance after SARS-CoV-2 infection

Obesity/diabetes decreases vaccine efficacy towards viral respiratory pathogens [13-19]. In humans receiving SARS-CoV-2 mRNA vaccination, those with obese/diabetic co-morbidity demonstrate the highest rates of severe disease and hospitalization [20-23]. Thus, to mimic the timing of vaccination in the general population, we assessed the efficacy of a clinically licensed adjuvanted protein subunit vaccine (NVX-CoV2373) vaccine in obese/diabetic mice. NVX-CoV2373 is an adjuvanted full-length Spike protein vaccine based on the SARS-CoV-2/Wuhan1 sequence that is highly effective at reducing SARS-CoV-2 infection in young ND mice[11]. At 18 weeks of age, ND and HFD mice were vaccinated with 1 µg of NVX-CoV2373 and then received a second dose 14 days later. On day 28 post-vaccination, blood was collected to evaluate neutralizing antibodies towards SARS-CoV-2 (MA10). On day 32 (~2 weeks after 2nd vaccination), mice were challenged with $1x10^5$ pfu/mouse of SARS-CoV-2 (MA10) (Figure 5A). As this dose has previously been shown to be lethal in obese/diabetic mice by 7 dpi (Figure 2A), mice were analyzed through 4dpi. We monitored weight daily and analyzed lungs on 2 and 4 dpi to determine viral lung titer and immune responses (Figure 5A). As expected, the unvaccinated mice had no detectable neutralizing antibodies against MA10 (Figure 5B). Vaccinated ND mice had ~ $1x10^4$ neut99, as did the vaccinated HFD mice (Figure 5B), demonstrating no difference between groups. Next, we observed that non vaccinated mice in both ND or HFD mouse groups had around a 50% survival rate by day 3, with no further mortality through 4dpi (Figure 5C). Unvaccinated ND mice lost 10% of their starting weight through 4dpi (Figure 5D), which was prevented with vaccination. However, vaccination in HFD mice did not protect from a ~10% starting weight loss by 4dpi.

Lungs of infected mice were next analyzed for viral titer at 2 and 4dpi. The unvaccinated ND mice had a viral titer of ~10^{10} pfu/g (Figure 5F) and other than 2 mice with moderate levels in their lungs, cleared the virus by 2dpi. By 4dpi, the unvaccinated ND mice had 2 logs lower virus compared to 2 dpi, and the vaccinated ND mice had almost no detectable virus in their lungs (Figure 5F). For the HFD mice, at 2 dpi, there was little difference in lung titer between vaccinated and unvaccinated mice even though these mice had equivalent levels of neutralizing antibody (Figure 5F). At 4dpi, the unvaccinated HFD mice had equivalent lung titers to the ND mice, and the vaccinated HFD mice had no detectable

virus in their lungs (Figure 5F). This demonstrates that despite comparable neutralizing titers in vaccinated HFD and ND mice, there is significantly delayed clearance of SARS-CoV-2 in obese/diabetic mice.

HFD mice have increased neutrophil infiltration and higher inflammatory chemokine response after SARS-CoV-2 infection

Our data demonstrating that HFD mice suffer from increased weight loss and have delayed clearance suggests they have a distinct immune response that alters infection. To assess the innate immune response of HFD mice after challenge with SARS-CoV-2, we performed both flow cytometry based immunophenotyping and quantification of cytokine and chemokine protein levels in the lungs. As they are part of the initial response to infection, we first quantified neutrophils in the lungs. On day 2 post-challenge, we observed that vaccinated HFD mice have higher numbers of neutrophils as compared to vaccinated ND mice (Figure 6A). By day 4 post-challenge, we observed a reduction in total number of neutrophils in vaccinated mice compared to unvaccinated, and again higher numbers of neutrophils in obese/diabetic mice compared to their controls (Figure 6A). When we examined $CD11b^+$, monocyte-derived, $CD103^+$, and plasmacytoid dendritic cells, we did not observe any differences between ND and HFD mice at either 2 or 4dpi. (Figure 6 B-E). When we examined natural killer cells, the ND mice had higher levels compared to HFD sham vaccinated mice at 4 dpi (Figure 7A).

We next wanted to examine the cells of the adaptive immune system by analyzing the lung's B and T cell response. We did not observe differences in B cells ($CD19^+$) numbers between groups (Figure 7E). When we examined the cell-mediated immune response, we found a difference in T cell response. When we examined the overall $CD3^+$ T cell response, we observed an expansion at 4dpi in the ND vaccinated mice compared to unvaccinated (Figure 7B). This expansion was not observed in the HFD mice. We did observe an expansion of T helper cells ($CD4^+$ cells) in the HFD vaccinated mice compared to unvaccinated mice (Figure 7C). Interestingly, we observed that unvaccinated HFD mice had fewer cytotoxic $CD8^+$ T cells compared to ND unvaccinated suggesting an altered T cell profile that may play a part in the clearance phenotype we observed.

We next performed a multiplexing cytokine assay to examine the concentration of soluble immune mediators in the lungs of vaccinated ND and HFD SARS-CoV-2 infected mice. When we compared the ND and HFD mice at 2 dpi, we observed higher levels of CCL2, CCL5, CCL7, CXCL10, and IL-6, and at 4dpi, CCL2, CCL5, CXCL12, CXCL1, GM-CSF, and TNF-α in HFD mice compared to ND mice

(Figure 8). These chemokines are all produced from or attract neutrophils and are concordant with the increased neutrophil infiltration we observe in flow cytometry analysis of infected mice.

Discussion

SARS-CoV-2 infection is more severe in obese and diabetic individuals[2-4, 8]. This has been observed in epidemiological data across many countries and economic levels[5]. Increased disease in diabetic and obese individuals is seen following several viral infections, including Influenza virus, Hepatitis B, Hepatitis C, and another highly pathogenic coronavirus, MERS-CoV[7, 27, 28]. We have previously demonstrated that in a mouse model of MERS-CoV, there is increased inflammation and a dysregulated immune response[6]. In this work, we utilized an obese and diabetic mouse model for the study of SARS-CoV-2 pathogenesis to determine whether we could observe increased disease as well as assess the effect of obesity and diabetes on SARS-CoV-2 vaccine responses.

We find that there are significant differences in the obese and diabetic (HFD) mice compared to normal mice after SARS-CoV-2 infection. First, the HFD mice have increased mortality after SARS-CoV-2 infection compared to ND mice. There are no observed differences in lung pathology or virus titer to explain the reason for the mortality other than the increased neutrophil infiltration we observed in the lungs of mice, which may have an overreaching effect on other aspects of host response not accounted for in this work.

Upon vaccination of the ND and HFD mice, we identify severe effects of obesity and diabetes on the vaccine mediated protection in mice. While neutralizing antibody levels are similar between ND and HFD mice and lethality is protected in both the ND and HFD vaccinated mice, even with their advanced age to the initial testing, there is no protection from weight loss in the vaccinated HFD mice compared to ND mice. When virus levels in the lung were analyzed, we observe a significant delay in clearance of virus at 2 dpi with the HFD mice showing no reduction in virus titer of vaccinated mice while the ND mice reduce virus titer by 4 logs in lungs at the same timepoint. Analysis of the inflammatory response in the mice also shows differences with the key difference being higher levels of neutrophils in the lungs of sham and vaccinated HFD mice compared to ND mice. This was corroborated by assaying for chemokines and cytokines in these lungs. We find that neutrophil produced chemokines and cytokines are significantly upregulated in the HFD mice, potentially associated with the reduction in clearance of virus from HFD vaccinated mice.

We interpret these results to demonstrate that the HFD mouse model reflects what is seen in humans with obesity and diabetes throughout the COVID-19 pandemic. This comorbid population has

significantly more hospitalizations, irrespective of vaccine status. This model also allows us to begin to differentiate the mechanism behind this lack of protection from SARS-CoV-2. With equivalent neutralizing antibody levels but less clearance in lungs, we hypothesize that this is due to changes in quality of the antibodies produced. Potentially the antigens that the antibodies recognize, or the subtypes of the antibodies are changed in the obese/diabetic mice compared to normal mice. We also observe the strong association of a hyperactive neutrophil response in the lungs. This could either be due to increased neutrophil recruitment or once there the neutrophils are not responding correctly. Both of these possibilities are being assessed in various mouse models of neutrophil dysregulation.

We hypothesize that the dysregulated immune response leads to increased morbidity and mortality as well as skewing the ability of antibodies produced by vaccination to clear viral infection. It is yet to be determined whether it is the metabolic disease associated with obesity that is driving this response or the hyperglycemia of type 2 diabetes. We are currently evaluating various additional models of these diseases to determine molecular mechanisms that exacerbate SARS-CoV-2 pathogenesis and this will allow us to test therapeutic agents for these and other comorbidities.

Methods

Cells and Virus Strain:

Virus and cells were processed as described previously [29]. Briefly, Vero E6 cells (ATCC# CRL 1586) were cultured in DMEM (Quality Biological), supplemented with 10% (v/v) fetal bovine serum (Gibco), 1% (v/v) penicillin/streptomycin (Gemini Bio-products) and 1% (v/v) L-glutamine (2 mM final concentration, Gibco) (Vero media). Cells were maintained at 37°C and 5% CO_2. SARS-CoV-2 (MA10) was provided by Dr. Ralph Baric (UNC). Stocks were prepared by infection of VeroE6 cells for two days when CPE was starting to be visible [30]. Media were collected and clarified by centrifugation before being aliquoted for storage at −80°C. The stock titer was determined by plaque assay using Vero E6 cells as described previously [31]. All work with infectious virus was performed in a Biosafety Level 3 laboratory and approved by our Institutional Biosafety Committee.

Animal Ethics Statement:

The University of Maryland School of Medicine is accredited by the Association for Assessment and Accreditation of Laboratory Animal Care (AAALAC International). All animal procedures were in accordance with NRC Guide for the Care and Use of Laboratory Animals, the Animal Welfare Act, and the CDC/NIH Biosafety in Microbiological and Biomedical Laboratories. Mouse studies were approved

by The University of Maryland School of Medicine IACUC. Studies were conducted in accordance with the National Institutes of Health Guide for Care and Use of Laboratory Animals (NIH publication 8023, Revised 1978). All mouse infections are carried out in an animal BSL-3 facility in accordance with approved practices.

Mouse Infections:

18-weeks-old male C57BL/6 diet included obesity (DIO) and C57BL/6 control mice were purchased from Jackson Laboratory. On day 0, mice were anesthetized by intraperitoneal injection 50 µL of a mix of xylazine (0.38 mg/mouse) and ketamine (1.3 mg/mouse) diluted in phosphate-buffered saline (PBS). While anesthetized, mice were intranasally inoculated with either 50 µL sterile PBS, 1 x 10^3 PFU or 1x10^5 PFU of SARS-CoV-2 MA10. Mice are monitored daily for weight loss and signs of morbidity. On days 2, 4, and 7, animals were euthanized, and lung tissue was collected for further analysis.

Mouse Challenge Study:

18-weeks-old male C57BL/6 diet included obesity (DIO) and C57BL/6 control mice were purchased from Jackson Laboratory and immunized by intramuscular (IM) injection with two doses spaced 14 days apart (day 0 and 14) of 1 µg rS-WU1, with 5 µg saponin-based Matrix-M™ adjuvant (Novavax, AB, Uppsala, SE) as a prime/boost. A placebo group was injected with vaccine formulation buffer as a negative control. Serum was collected for analysis on days 0 and 28. Vaccinated and control animals were intranasally challenged with SARS-CoV-2 on study day 32. On days 2 and 4 post-challenge, animals were euthanized, and lung tissue was collected for further analysis.

Histology & Immunohistochemistry:

Lung sections were fixed in 4% paraformaldehyde (PFA) in phosphate-buffered saline (PBS) for a minimum of 48 h, after which they were sent to the Histology Core at the University of Maryland, Baltimore, for paraffin embedding and sectioning. Five-micrometer sections were prepared and used for hematoxylin and eosin (H&E) staining by the Histology Core Services.

For SARS-CoV-2 nucleocapsid immunohistochemistry staining, five-micrometer sections were cut from paraffin-embedded blocks and placed onto positively charged slides. The sections were immunostained using the Dako EnVision FLEX + detection system (DAKO, Carpinteria, CA). The Dako PT link was used for deparaffinization and heat-induced epitope retrieval using Dako Target Retrieval Solution, High pH, for 20 minutes. Endogenous peroxidase activity was blocked with DAKO Peroxidase-Blocking Reagent for 5

min before incubation with rabbit polyclonal SARS Nucleocapsid Protein Antibody [NB100-56576] (Novus Biologicals, Centennial, CO), 1:400 for 20 minutes at room temperature, followed by DAKO Anti-rabbit HRP Detection Reagent for 20 minutes. Finally, the sections were incubated for 10 min with DAKO diaminobenzene (DAB) before they were counterstained with Dako FLEX hematoxylin, rinsed, and mounted in Cytoseal XYL (Thermo Scientific, Waltham, MA). Sections were imaged at 10x magnification, and figures were put together using Adobe Photoshop and Illustrator software (Adobe, San Jose,CA).

Plaque Assay:

VeroE6/TMPRSS2 cells were cultured in DMEM (Quality Biological), supplemented with 10% (v/v) heat-inactivated fetal bovine serum (Sigma), 1% (v/v) penicillin/streptomycin (Gemini Bio-products), and 1% (v/v) L-glutamine (2 mM final concentration, Gibco) (Vero Media). Cells were maintained at 37°C (5% CO_2). SARS-CoV-2 lung titers were quantified by homogenizing mouse lungs in 1ml phosphate-buffered saline (PBS; Quality Biological Inc.) using 1.0mm glass beads (Sigma Aldrich) and a Beadruptor (Omni International Inc). VeroE6 cells are plated in 12 well plates with $1.5x10^5$ cells per well. SARS-CoV-2 virus titer in plaque forming units was determined by plaque assay. In the plaque assay, 25 µl of the lung homogenate is added to 225 µl of DMEM and diluted 10-fold across a 6-point dilution curve with 200ul of diluent added to each well. After 1 hour, a 2 ml agar overlay containing DMEM is added to each well. Plates are incubated for three days at 37°C (5% CO_2) before plaques are counted.

SARS-CoV-2 Neutralization Titer Determination:

SARS-CoV-2 neutralizing antibody titers were determined as described previously [32]. Briefly, serum samples were heat-inactivated to remove complement and allowed to equilibrate to room temperature before processing. Samples were diluted in duplicate for a 12-point, 1:2 dilution series with an initial dilution of 1:40 dilution (1:80 following virus addition). Dilution plates were then transported into the BSL-3 laboratory, and equal volume SARS-CoV-2 inoculum was added to each plate. A non-treated, virus-only control and a mock infection control were included on every plate. The sample/virus mixture was then incubated at 37°C (5.0% CO_2) for 1 hour before transferring to 96-well titer plates with confluent VeroE6 cells. Titer plates were incubated at 37°C (5.0% CO_2) for 72 hours, followed by CPE determination for each well in the plate. The first sample dilution to show CPE was reported as the minimum sample dilution required to neutralize >99% of the concentration of SARS-CoV-2 tested (neut99).

Gene Expression:

Mouse lung tissue was homogenized in 1 mL of TRIzol (Ambion) using 1.4-mm glass beads (Omni International, Inc.) and a beadruptor (Omni International, Inc.) RNA was extracted using the DIRECT-zol Mini RNA Extraction kit (Zymo Research) per the manufacturer's instructions. RNA was transcribed into cDNA using RT^2 First Strand Kit (Qiagen). Gene expression was performed using Real-time PCR for RT^2 Profile PCR Array Mouse Cytokine and Chemokines using RT^2 SYBR® Green Mastermixes (Qiagen). Using the RT^2 qPCR Array Data Analysis spreadsheet, gene expression was calculated using the ΔΔCt method with house keeping genes as the control, and fold-change calculated relative to control mice infected lungs. Fold-regulation, which represents fold-change in a biologically meaningful way, was calculated using fold change. A fold-change value greater than one indicates an up-regulation, and the fold-regulation is equal to the fold change. A fold-change value less than one indicates a down-regulation, and the fold-regulation is negative inverse of the fold-change.

Cytokine and Chemokine Quantification:

For the quantification of secreted cytokine and chemokines induced by SARS-CoV-2 infection, mice lung tissue was homogenized in 1 mL of PBS (Quality Biologicals, Inc.) using 1.4-mm glass beads (Omni International, Inc.) and a beadruptor (Omni International, Inc.). Bio-Plex Pro Mouse Chemokine Panel 31-plex (BIORAD) was used to quantify cytokines and chemokines in lung homogenate according to the manufacturer's protocol with the addition of a fixation step after the final wash. Samples underwent a 24-hour fixation (4 % formaldehyde, Sigma-Aldrich) at 4°C. After fixation, the plate was washed three times in wash buffer, microparticles were resuspended in 100 µL wash buffer, and analyzed on a Luminex MagPix and xPONENT Software version 4.3. Based on the standard curve, concentrations (pg/mL) of each analyte were calculated for all samples.

Flow Cytometry:

Single cells were isolated from lungs using the Lung Dissociation Kit, mouse and gentleMACS Dissociator (Miltenyi Biotec). Lungs were placed in C tubes (Miltenyi Biotec) containing 2.2 mL Buffer S, 15 µL of Enzyme A, and 100 µL of Enzyme D. Lungs were run on m_lung_01 and allowed to digest for 30 minutes at 37°C followed by running m_lung_02. Cell suspensions were filtered on a 70-µm filter (BD), and cells were pelleted by centrifugation. Red blood cells were lysed in ammonium-chloride-potassium lysis buffer (Quality Biological, Inc.) and subsequently washed with PBS containing 3% FBS. Approximately, $1x10^6$ cells were plated and washed twice with PBS containing. Cells were stained for viability using the

Live/Dead Fixable NIR Dead Cell Stain Kit (Molecular Probes). Cells were washed with PBS containing 3% FBS. Cells were stained with antibody cocktails made in BD Horizon Brilliant Stain Buffer (BD). The antibodies used were as follows: CD45 Alexa Fluor 700 (BioLegend, clone 30-F11), CD11b Brilliant Violet 650 (BioLegend, clone M1/70), Ly6G Brilliant Violet 785 (BioLegend , clone 1A8), Ly6C Brilliant Violet 510 (BioLegend, clone HK1.4), CD3 BUV 563 (BD, clone 145-2C11), CD4 FITC (BioLegend, clone GK1.5), CD8a APC (BioLegend clone 53-6.7), CD19 PE (BioLegend clone 6D5), and NK1.1 Pacific Blue (BioLegend, clone PK136), CD65 Brilliant Violet 605 (BioLegend, clone X54-5/7.1), CD103 BUV 661 (BD, clone 2e7), Siglec-H BUV 563 (BD, clone 440c), and Siglec-F Brilliant Violet 711 (BD, clone E50-2440). Stained cells were washed twice and fixed for 1 hour in FluoroFix (BioLegend). Fixed cells were washed once in PBS containing 3% FBS and resuspended in PBS containing 3% FBS. Samples were acquired (approximately 250,000 events) using the Aurora-UV spectral flow cytometer (Cytek), and data were analyzed using FCS Express analysis software (DeNova Software, Pasadena, CA).

Statistical Analysis:

Statistical analyses were performed with GraphPad Prism 9.2 software (GraphPad Software, San Diego, CA). Data were analyzed using unpaired t-test, Log-rank (Mantel-Cox) test, one-way or two-way ANOVA followed by Tukey, Sidak, or Dunnett multiple comparison post-hoc test as indicated. All statistical analysis were two-sided and a $p < 0.05$ was consisted as statistically significant.

Competing/Conflict of Interest

M.B.F. is on the scientific advisory board of Aikido Pharma and has collaborative research agreements with Novavax, AstraZeneca, Regeneron, and Irazu Bio. These do not have any effect on the planning or interpretations of the work presented in this manuscript. N.P. and G.S are employees of Novavax.

Financial Support

This work is partially funded by BARDA #ASPR-20-01495, NIH R01 AI148166, NIH HHSN272201400007C, NIH HHSN272201400008C/ 0258-0689-4609 to M.B.F. RJ is funded by T32AI007524. N.P. and G.S are employees of and funded by Novavax.

Figure Legends

Figure 1: A high fat diet induces obesity and diabetes in C57BL/6J mice.

A. Schematic overview illustrating diet schedule and infection for control and obese/diabetic mice. Briefly, at weaning (3 weeks), mice were placed on a normal diet (ND) or high fat diet (HFD). At 18 weeks of age, these mice were infected with either $1x10^3$ or $1x10^5$ pfu of SARS-CoV-2 Mouse Adaptive 10, monitored daily for weight changes, and a subset was euthanized at day 2, 4, and 7 to analyze lung viral titer and host immune response. The **B.** fasted blood glucose concentration and **C.** fasted serum insulin were determined prior to infection *n=13* mice/group. These values were used to assess **D.** insulin resistance by HOMA-IR score {HOMA-IR = [26 * serum insulin (ng/ml) * blood glucose (mg/dL)]/405}. The **E.** starting weight of ND and HFD mice prior to infection *n=45* mice/group. * $p < 0.5$ and **** $p < 0.0001$ as determined by an unpaired two-sided t-test. The data are presented as mean ± SD.

Figure 2: Enhanced mortality in obesity/ diabetes mice after SARS-CoV-2 infection.
The **A.** survival, percent weight loss for **B.** low dose, **C.** high dose, grams lost for **D.** low dose, and **E.** high dose. **D.** Viral lung titers were assessed for control and obese/ diabetic mice throughout a SARS-CoV-2 MA10 infection. For **A.** * $p < 0.05$ as determined by a Log-rank (Mantel-Cox) test for survival analysis between ND and HFD for low and high infection dose with the data presented as mean ± SD with *n=10* mice/group. For **B-D** the data are presented as mean ± SD with *n*=3-5 mice/group.

Figure 3: Similar lung histology and viral clearance in control and obese/ diabetic mice.
Control and obese/diabetic mice were infected intranasally with either $1x10^3$ or $1x10^5$ pfu/ mouse. Lungs were collected on 2, 4, and 7 dpi and fixed in 10% neutral buffered formalin for greater than 24 hours. Tissue was embedded in paraffin. **A.** 5 µm sections were cut and stained with hematoxylin and eosin, and **B.** immunostained with anti-SARS Nucleocapsid Protein antibody. Images are shown at original magnification x10 and are representative of *n* = 3-5 mice/group.

Figure 4: Increased neutrophil recruitment, activation, and growth factor in infected HFD mice.
For the $1x10^3$ infectious dose, lung cytokine, chemokine, and growth factors were assessed at 2, 4, and 7 dpi using a mouse cytokine/chemokine array. The fold change was calculated compared to ND infected mice. For a fold change greater than one, the fold-regulation is the same, but for a fold change less than one, the fold regulation is the negative inverse of the fold-change. *n*=3 mice/group.

Figure 5: Viral clearance is delayed in obese/ diabetic vaccinated mice.

A. Schematic overview illustrating vaccination and challenge for ND and HFD mice. Briefly, at 18 weeks of age, mice were vaccinated as well as 14 days later. On day 28 post-vaccination, mice were bled to determine **B.** serum neutralizing antibodies prior to infection, *n* = 12-15 mice/group. On day 32, these mice were challenged with $1x10^5$ pfu of SARS-CoV-2 MA 10, monitored daily for weight changes, and a subset was euthanized on day 2 and 4 to analyze lung viral titer and host immune response. The **C.** mortality, weight loss of **D.** ND, **E.** HFD, and **F.** viral titer of sham and vaccinated mice after SARS-2 MA10 challenge. *n*= 5-10 mice/group. For **D**, * p <0.5 and *** p < 0.001 as determined by a mixed-effect analysis followed by a Sidak test for multiple comparisons. For **F.** p *** < 0.001 and p **** < 0.0001, data were log-transformed and analyzed by mixed-effect analysis followed by Sidik for multiple comparisons. The data are pooled from 2 independent experiments and presented as mean ± SD.

Figure 6: Increased neutrophil recruitment in the lungs of HFD mice after SARS-CoV-2 challenge. After SARS-2 MA10 challenge, lungs were harvested, cells isolated, and stained for surface markers for **A.** neutrophils, **B.** $CD11b^+$ DCs, **C.** monocyte-derived DCs, **D.**$CD103^+$ cDCs, **E.** plasmacytoid DCs at day 2 and 4 post-challenge. * p < 0.05 and ** p < 0.01 as data were log-transformed and analyzed by mixed-effect analysis followed by Tukey for multiple comparisons *n*=3-5 mice/group.

Figure 7: T cell dysregulation in the lungs of HFD mice after SARS-CoV-2 challenge. After SARS-2 MA10 challenge, lungs were harvested, cells isolated, and stained for surface markers for **A.** Natural Killer cells, **B.** Total T cells, **C.** T helper cells, **D.** Cytotoxic T cells, and **E.** B cells at day 2 and 4 post-challenge. * p < 0.05 as data were log-transformed and analyzed by mixed-effect analysis followed by Tukey for multiple comparisons *n*=3-5 mice/group

Figure 8: Increased neutrophil recruitment and cytokine production in HFD vaccinated mice after challenge. On day 2,4,7 dpi, lungs were harvested and used in a Bio-plex pro mouse chemokine panel. The pg/mL was generated from a standard curve. * p < 0.05 and ** p < 0.01 as analyzed by mixed-effect analysis followed by Sidak for multiple comparisons *n*=3-5 mice/group.

References

1. CDC. *National Diabetes Statistics Report*. Available from: https://www.cdc.gov/diabetes/data/statistics-report/index.html.

2. Kompaniyets, L., et al., *Body Mass Index and Risk for COVID-19-Related Hospitalization, Intensive Care Unit Admission, Invasive Mechanical Ventilation, and Death - United States, March-December 2020.* MMWR Morb Mortal Wkly Rep, 2021. **70**(10): p. 355-361.
3. Apicella, M., et al., *COVID-19 in people with diabetes: understanding the reasons for worse outcomes.* Lancet Diabetes Endocrinol, 2020. **8**(9): p. 782-792.
4. Rawshani, A., et al., *Severe COVID-19 in people with type 1 and type 2 diabetes in Sweden: A nationwide retrospective cohort study.* Lancet Reg Health Eur, 2021. **4**: p. 100105.
5. Ozonoff, A., et al., *Phenotypes of disease severity in a cohort of hospitalized COVID-19 patients: Results from the IMPACC study.* EBioMedicine, 2022. **83**: p. 104208.
6. Kulcsar, K.A., et al., *Comorbid diabetes results in immune dysregulation and enhanced disease severity following MERS-CoV infection.* JCI Insight, 2019. **4**(20).
7. Yang, Y.M., et al., *Impact of Comorbidity on Fatality Rate of Patients with Middle East Respiratory Syndrome.* Sci Rep, 2017. **7**(1): p. 11307.
8. Alanazi, K.H., et al., *Diabetes Mellitus, Hypertension, and Death among 32 Patients with MERS-CoV Infection, Saudi Arabia.* Emerg Infect Dis, 2020. **26**(1): p. 166-168.
9. Badawi, A. and S.G. Ryoo, *Prevalence of Diabetes in the 2009 Influenza A (H1N1) and the Middle East Respiratory Syndrome Coronavirus: A Systematic Review and Meta-Analysis.* J Public Health Res, 2016. **5**(3): p. 733.
10. Guebre-Xabier, M., et al., *NVX-CoV2373 vaccine protects cynomolgus macaque upper and lower airways against SARS-CoV-2 challenge.* Vaccine, 2020. **38**(50): p. 7892-7896.
11. Tian, J.H., et al., *SARS-CoV-2 spike glycoprotein vaccine candidate NVX-CoV2373 immunogenicity in baboons and protection in mice.* Nat Commun, 2021. **12**(1): p. 372.
12. Leist, S.R., et al., *A Mouse-Adapted SARS-CoV-2 Induces Acute Lung Injury and Mortality in Standard Laboratory Mice.* Cell, 2020. **183**(4): p. 1070-1085 e12.
13. Paich, H.A., et al., *Overweight and obese adult humans have a defective cellular immune response to pandemic H1N1 influenza A virus.* Obesity (Silver Spring), 2013. **21**(11): p. 2377-86.
14. Kim, Y.H., et al., *Diet-induced obesity dramatically reduces the efficacy of a 2009 pandemic H1N1 vaccine in a mouse model.* J Infect Dis, 2012. **205**(2): p. 244-51.
15. Costanzo, A.E., et al., *Obesity impairs gammadelta T cell homeostasis and antiviral function in humans.* PLoS One, 2015. **10**(3): p. e0120918.
16. Fisher-Hoch, S.P., C.E. Mathews, and J.B. McCormick, *Obesity, diabetes and pneumonia: the menacing interface of non-communicable and infectious diseases.* Trop Med Int Health, 2013. **18**(12): p. 1510-9.
17. Hagau, N., et al., *Clinical aspects and cytokine response in severe H1N1 influenza A virus infection.* Crit Care, 2010. **14**(6): p. R203.
18. Painter, S.D., I.G. Ovsyannikova, and G.A. Poland, *The weight of obesity on the human immune response to vaccination.* Vaccine, 2015. **33**(36): p. 4422-9.
19. Tagliabue, C., et al., *Obesity: impact of infections and response to vaccines.* Eur J Clin Microbiol Infect Dis, 2016. **35**(3): p. 325-31.
20. Caimi, B., et al., *Sero-survey on long-term care facility residents reveals increased risk of sub-optimal antibody response to BNT162b2: implications for breakthrough prevention.* BMC Geriatr, 2022. **22**(1): p. 191.
21. Soetedjo, N.N.M., et al., *Antibody response following SARS-CoV-2 vaccination among patients with type 2 diabetes mellitus: A systematic review.* Diabetes Metab Syndr, 2022. **16**(2): p. 102406.
22. Anand, S., et al., *SARS-CoV-2 Vaccine Antibody Response and Breakthrough Infection in Patients Receiving Dialysis.* Ann Intern Med, 2022. **175**(3): p. 371-378.

23. Mitsunaga, T., et al., *The evaluation of factors affecting antibody response after administration of the BNT162b2 vaccine: a prospective study in Japan.* PeerJ, 2021. **9**: p. e12316.
24. Borriello, F., et al., *An adjuvant strategy enabled by modulation of the physical properties of microbial ligands expands antigen immunogenicity.* Cell, 2022. **185**(4): p. 614-629 e21.
25. Nanishi, E., et al., *An aluminum hydroxide:CpG adjuvant enhances protection elicited by a SARS-CoV-2 receptor binding domain vaccine in aged mice.* Sci Transl Med, 2022. **14**(629): p. eabj5305.
26. Dinnon, K.H., 3rd, et al., *SARS-CoV-2 infection produces chronic pulmonary epithelial and immune cell dysfunction with fibrosis in mice.* Sci Transl Med, 2022: p. eabo5070.
27. Almond, M.H., et al., *Obesity and susceptibility to severe outcomes following respiratory viral infection.* Thorax, 2013. **68**(7): p. 684-6.
28. Honce, R. and S. Schultz-Cherry, *Impact of Obesity on Influenza A Virus Pathogenesis, Immune Response, and Evolution.* Front Immunol, 2019. **10**: p. 1071.
29. Weston, S., et al., *Broad Anti-coronavirus Activity of Food and Drug Administration-Approved Drugs against SARS-CoV-2 In Vitro and SARS-CoV In Vivo.* J Virol, 2020. **94**(21).
30. Matsuyama, S., et al., *Enhanced isolation of SARS-CoV-2 by TMPRSS2-expressing cells.* Proc Natl Acad Sci U S A, 2020. **117**(13): p. 7001-7003.
31. Coleman, C.M. and M.B. Frieman, *Growth and Quantification of MERS-CoV Infection.* Curr Protoc Microbiol, 2015. **37**: p. 15E 2 1-9.
32. Keech, C., et al., *Phase 1-2 Trial of a SARS-CoV-2 Recombinant Spike Protein Nanoparticle Vaccine.* The New England journal of medicine, 2020. **383**(24): p. 2320-2332.

Figure 1

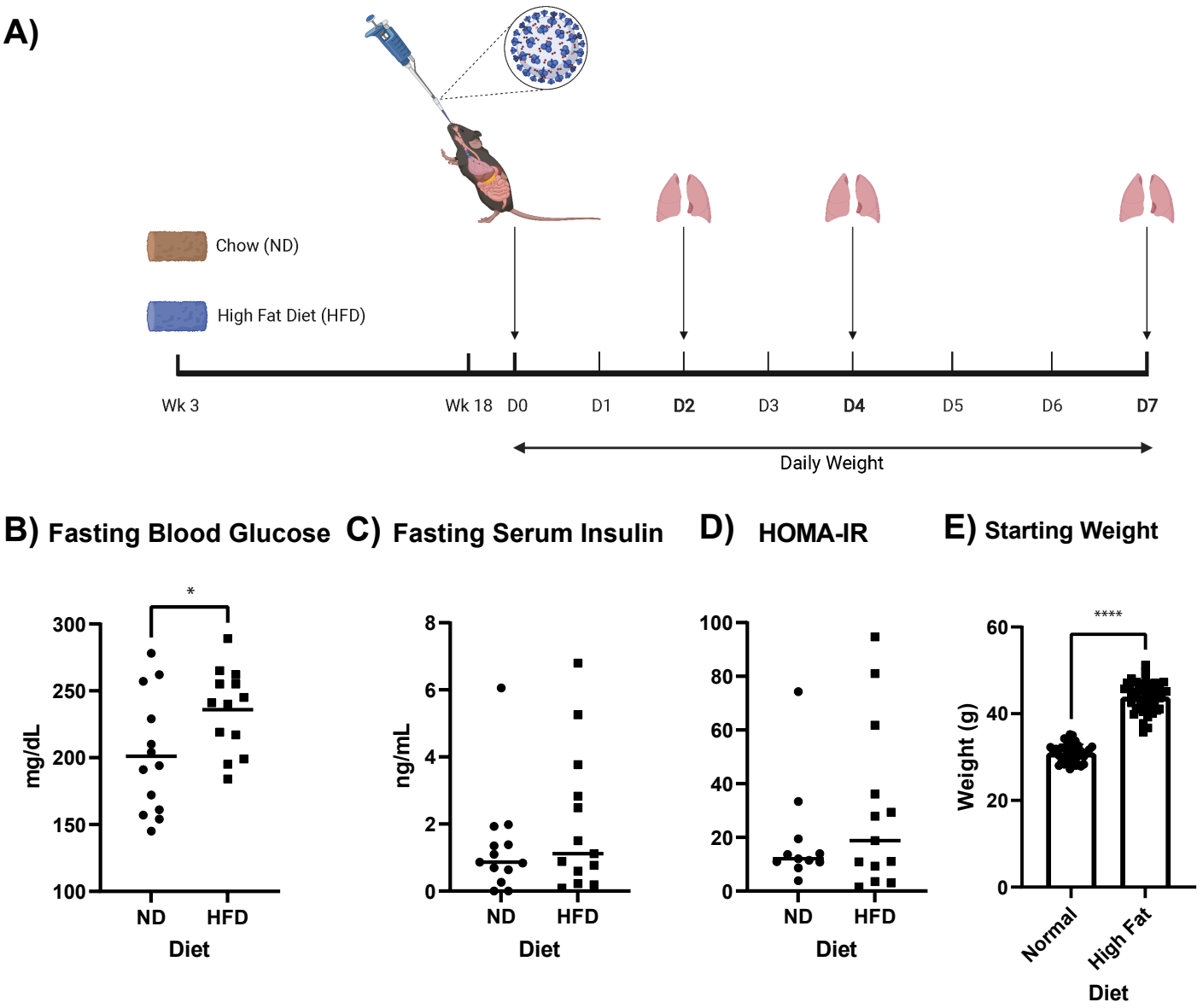
A)
Chow (ND)
High Fat Diet (HFD)
Wk 3
Wk 18
D0
D1
D2
D3
D4
D5
D6
D7
Daily Weight
B) Fasting Blood Glucose
mg/dL
300
250
200
150
100
*
ND
HFD
Diet
C) Fasting Serum Insulin
ng/mL
8
6
4
2
0
ND
HFD
Diet
D) HOMA-IR
100
80
60
40
20
0
ND
HFD
Diet
E) Starting Weight
Weight (g)
60
40
20
0
****
Normal
High Fat
Diet

Figure 2

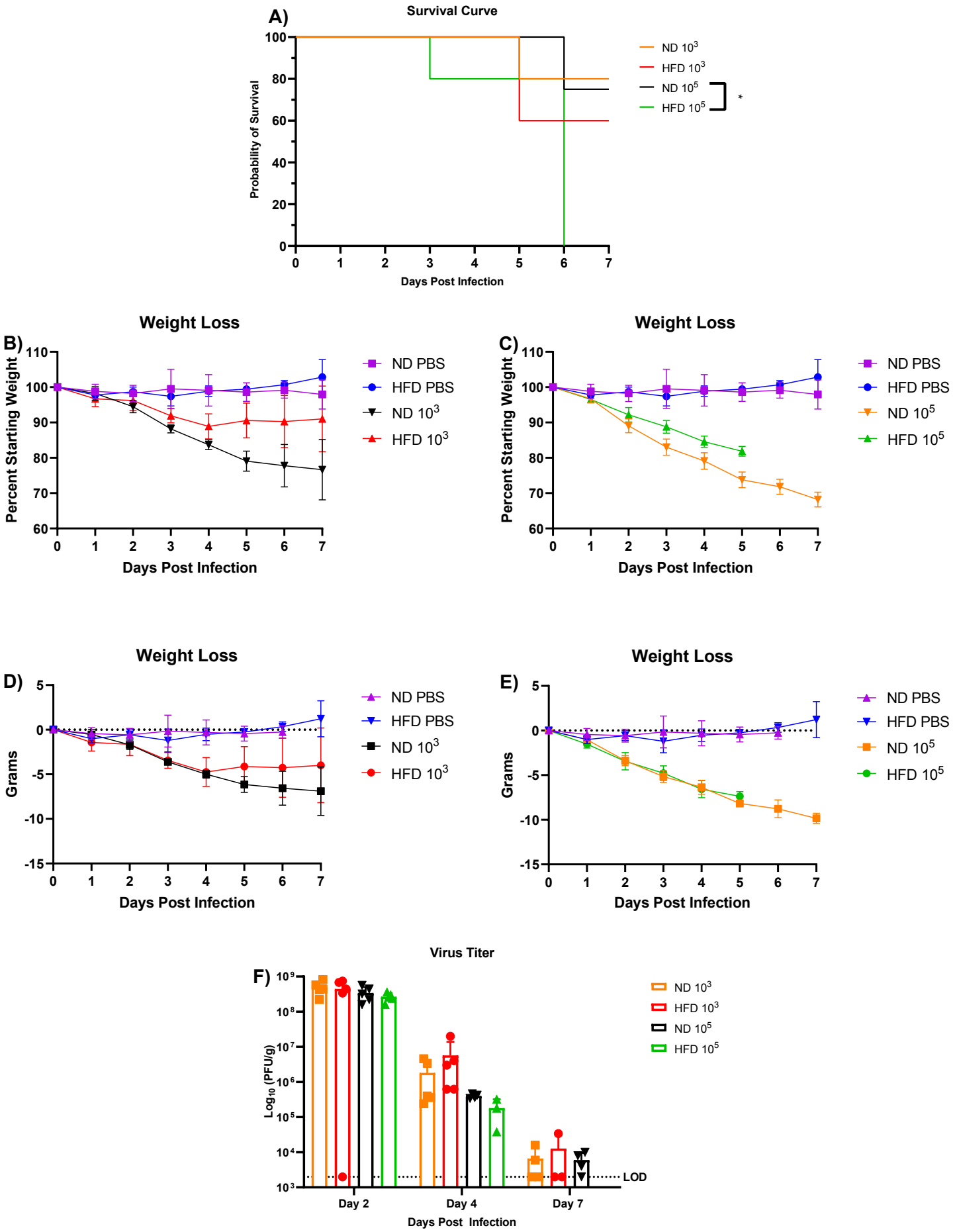
A)
Survival Curve
Probability of Survival
Days Post Infection
ND 10^3
HFD 10^3
ND 10^5
HFD 10^5
*
B)
Weight Loss
Percent Starting Weight
Days Post Infection
ND PBS
HFD PBS
ND 10^3
HFD 10^3
C)
Weight Loss
Percent Starting Weight
Days Post Infection
ND PBS
HFD PBS
ND 10^5
HFD 10^5
D)
Weight Loss
Grams
Days Post Infection
ND PBS
HFD PBS
ND 10^3
HFD 10^3
E)
Weight Loss
Grams
Days Post Infection
ND PBS
HFD PBS
ND 10^5
HFD 10^5
F)
Virus Titer
Log10 (PFU/g)
LOD
Day 2
Day 4
Day 7
Days Post Infection
ND 10^3
HFD 10^3
ND 10^5
HFD 10^5

Figure 3

A

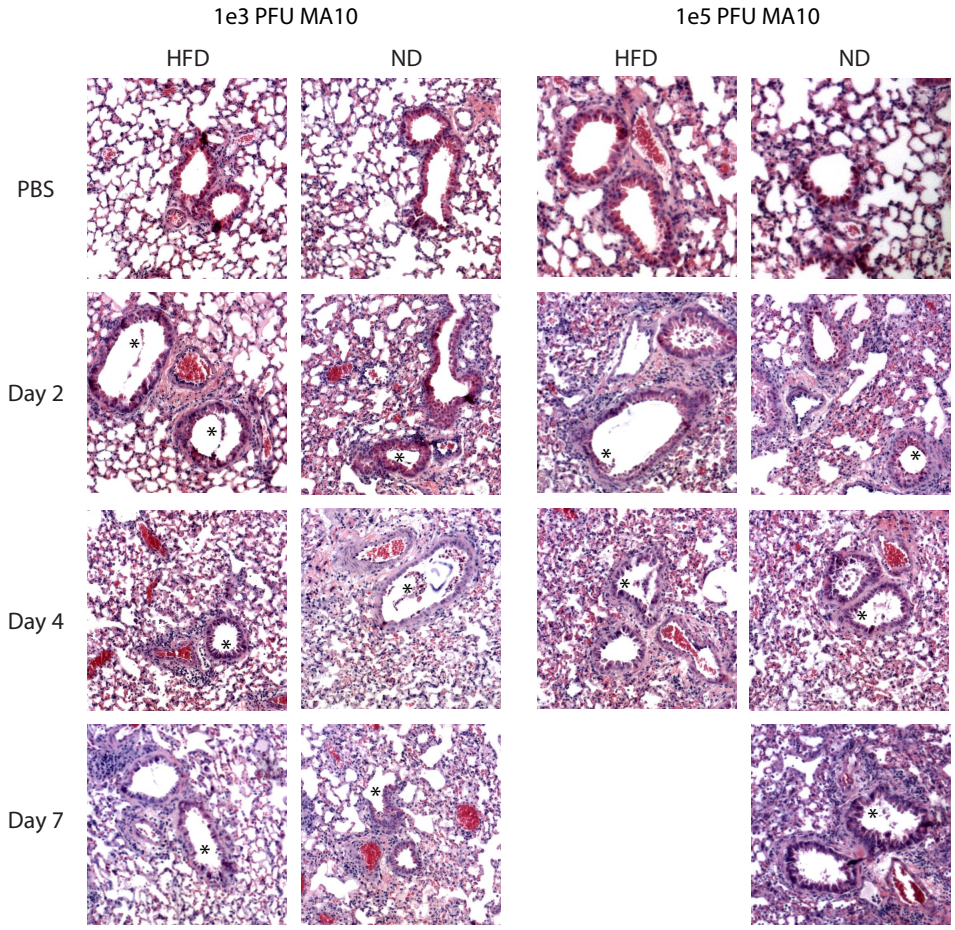
1e3 PFU MA10
1e5 PFU MA10
HFD
ND
HFD
ND
PBS
Day 2
Day 4
Day 7

B

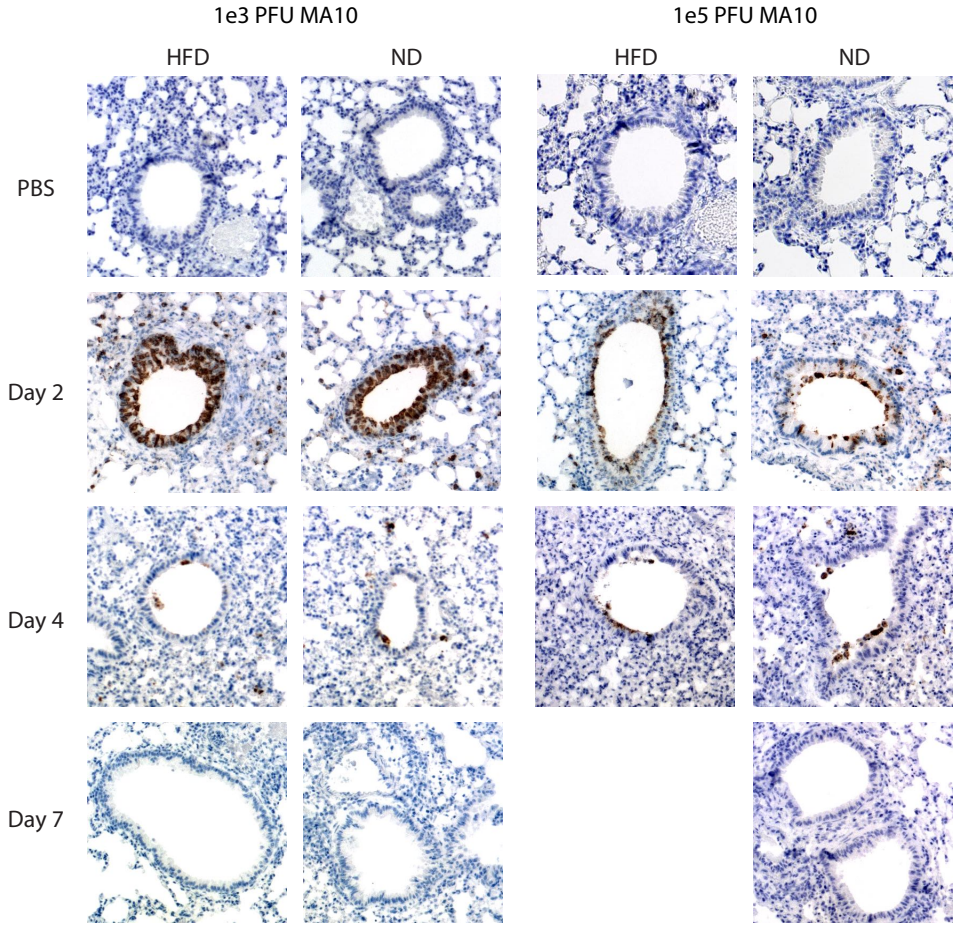
1e3 PFU MA10
1e5 PFU MA10
HFD
ND
HFD
ND
PBS
Day 2
Day 4
Day 7

Figure 4

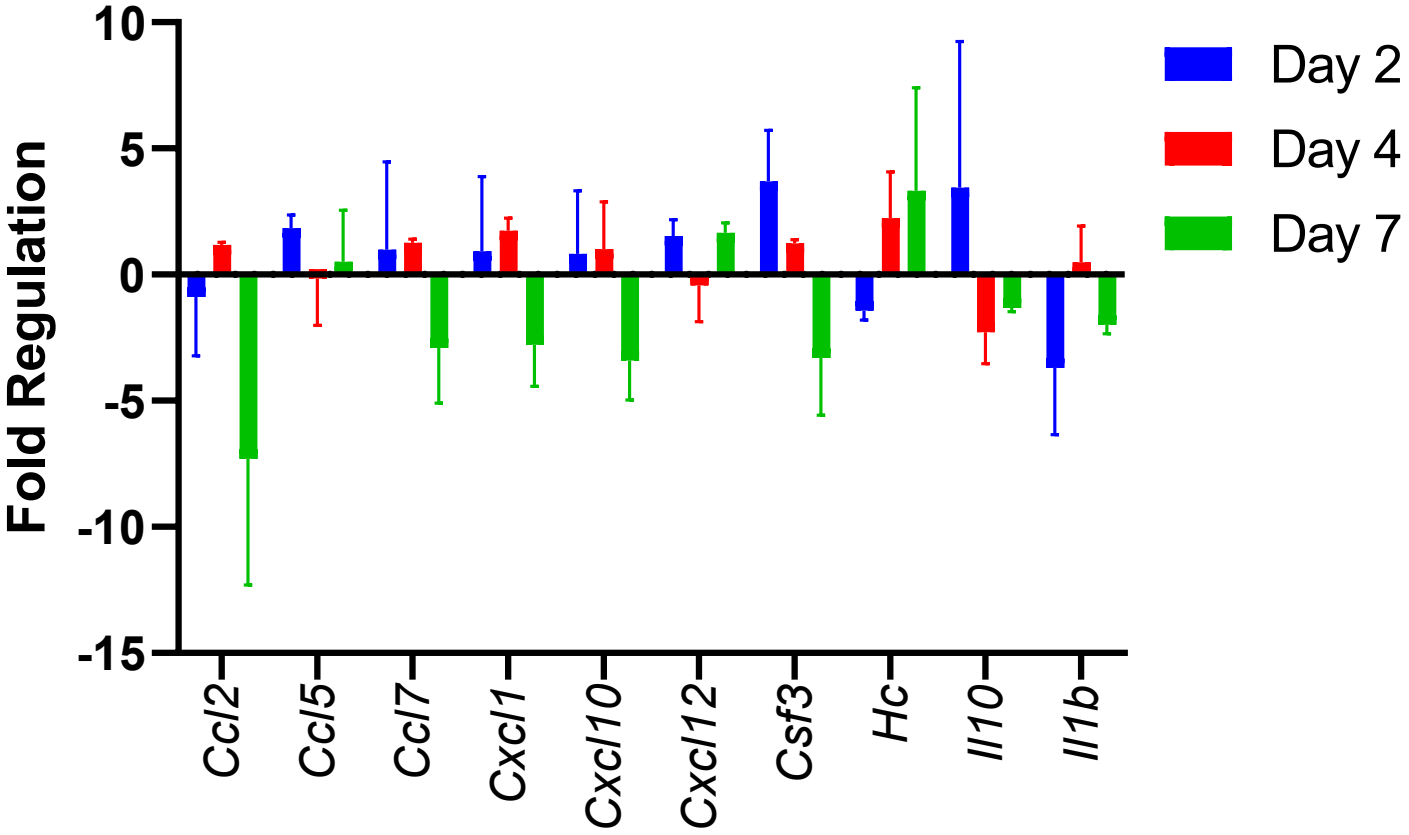
Fold Regulation
10
5
0
-5
-10
-15
Ccl2
Ccl5
Ccl7
Cxcl1
Cxcl10
Cxcl12
Csf3
Hc
Il10
Il1b
Day 2
Day 4
Day 7

Figure 5

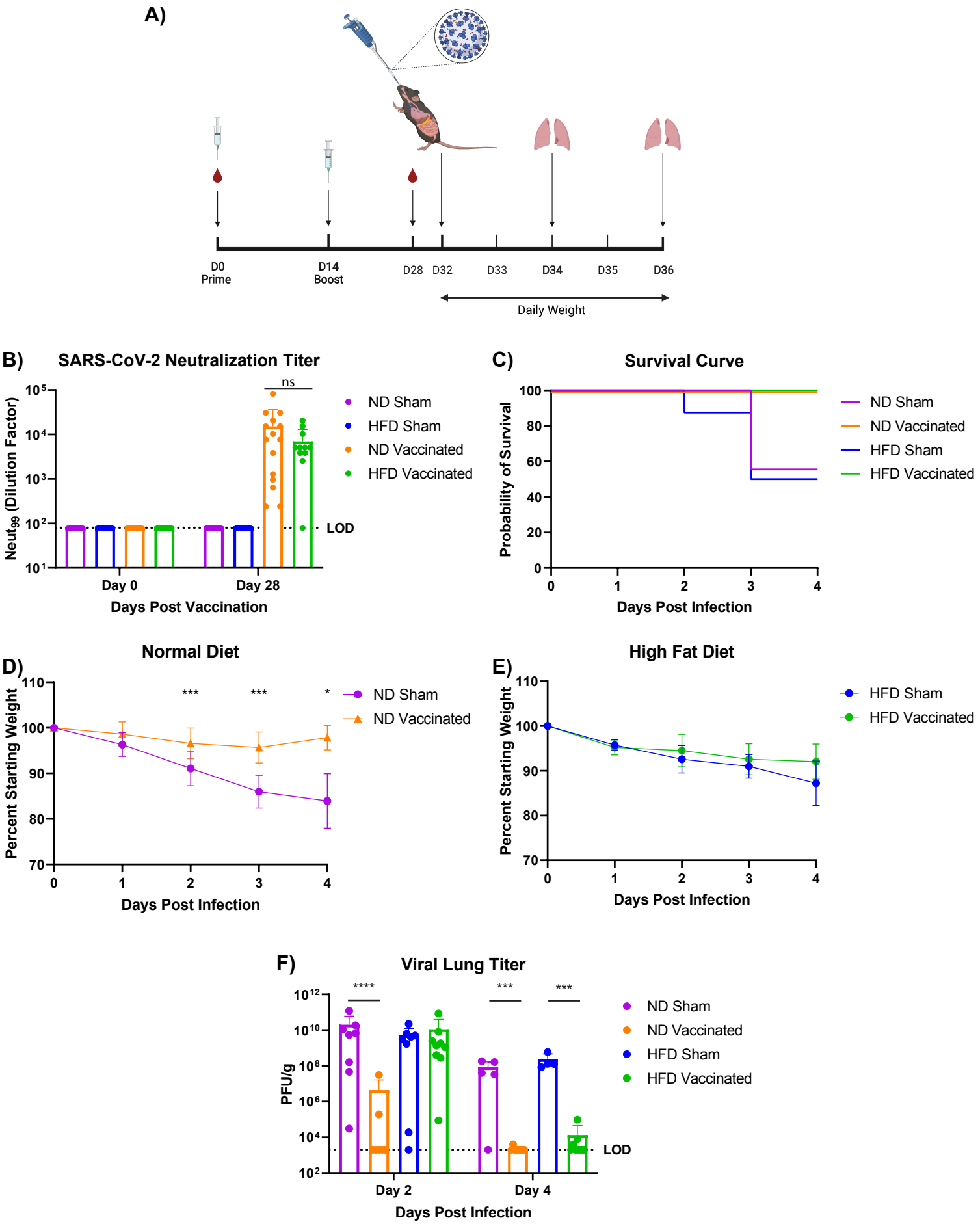
A)
D0
Prime
D14
Boost
D28
D32
D33
D34
D35
D36
Daily Weight
B)
SARS-CoV-2 Neutralization Titer
ns
Neut99 (Dilution Factor)
LOD
Day 0
Day 28
Days Post Vaccination
ND Sham
HFD Sham
ND Vaccinated
HFD Vaccinated
C)
Survival Curve
Probability of Survival
Days Post Infection
ND Sham
ND Vaccinated
HFD Sham
HFD Vaccinated
D)
Normal Diet
Percent Starting Weight
Days Post Infection
ND Sham
ND Vaccinated
E)
High Fat Diet
Percent Starting Weight
Days Post Infection
HFD Sham
HFD Vaccinated
F)
Viral Lung Titer
PFU/g
LOD
Day 2
Day 4
Days Post Infection
ND Sham
ND Vaccinated
HFD Sham
HFD Vaccinated

Figure 6

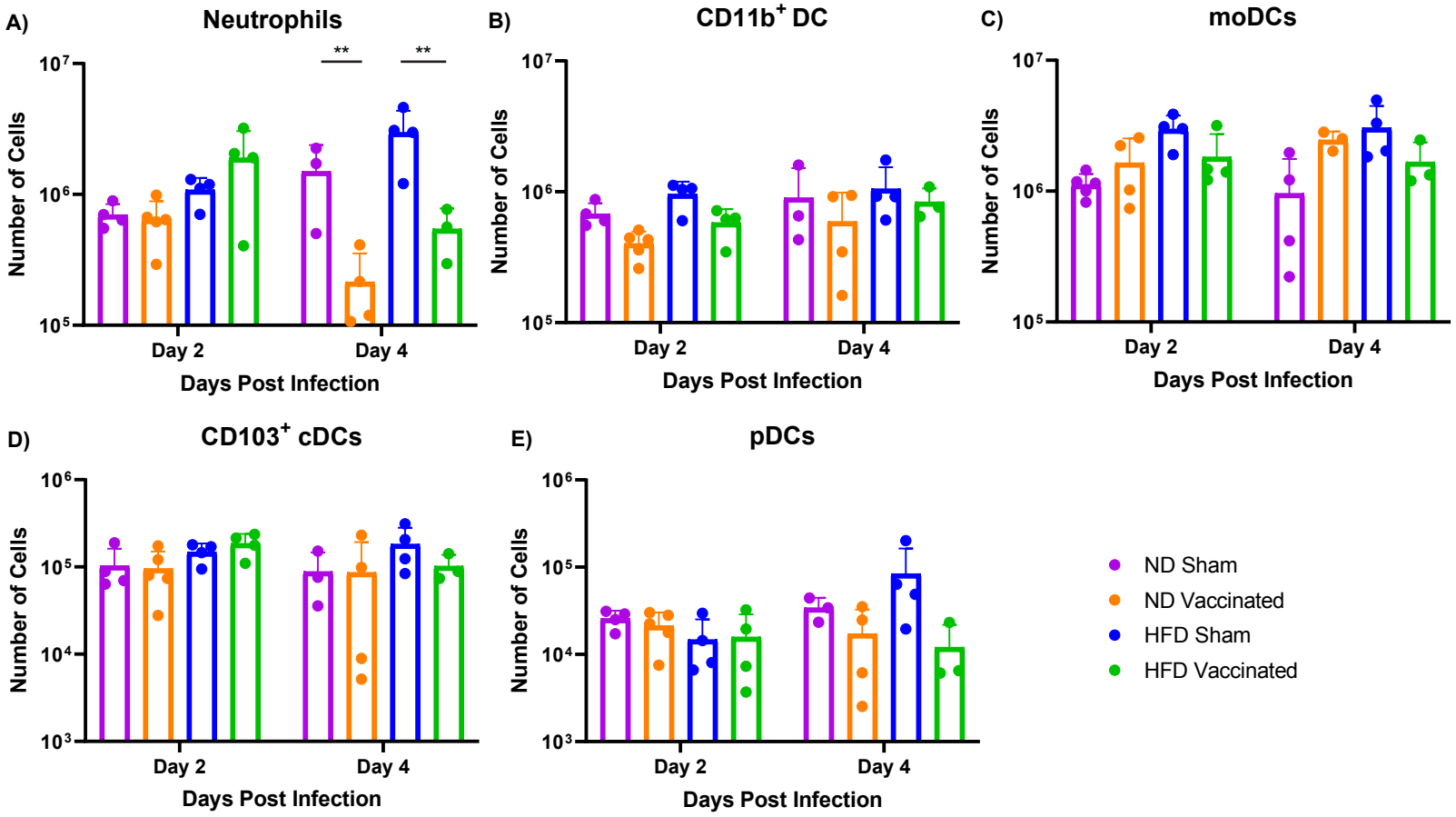
A)
Neutrophils
**
**
Number of Cells
10^7
10^6
10^5
Day 2
Day 4
Days Post Infection
B)
CD11b+ DC
Number of Cells
10^7
10^6
10^5
Day 2
Day 4
Days Post Infection
C)
moDCs
Number of Cells
10^7
10^6
10^5
Day 2
Day 4
Days Post Infection
D)
CD103+ cDCs
Number of Cells
10^6
10^5
10^4
10^3
Day 2
Day 4
Days Post Infection
E)
pDCs
Number of Cells
10^6
10^5
10^4
10^3
Day 2
Day 4
Days Post Infection
ND Sham
ND Vaccinated
HFD Sham
HFD Vaccinated

Figure 7

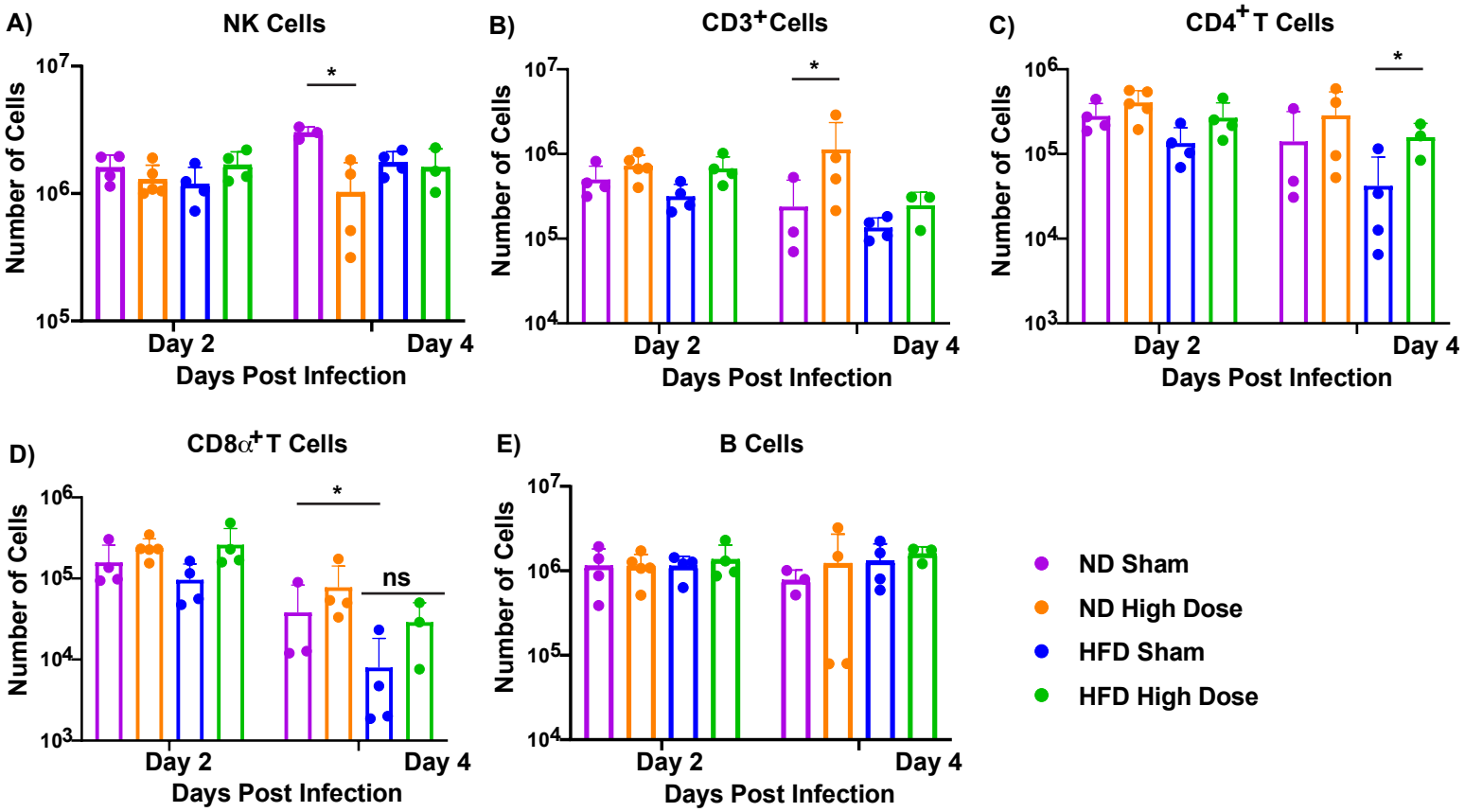
A)
NK Cells
Number of Cells
10^7
10^6
10^5
*
Day 2
Day 4
Days Post Infection
B)
CD3+Cells
Number of Cells
10^7
10^6
10^5
10^4
*
Day 2
Day 4
Days Post Infection
C)
CD4+ T Cells
Number of Cells
10^6
10^5
10^4
10^3
*
Day 2
Day 4
Days Post Infection
D)
CD8α+ T Cells
Number of Cells
10^6
10^5
10^4
10^3
*
ns
Day 2
Day 4
Days Post Infection
E)
B Cells
Number of Cells
10^7
10^6
10^5
10^4
Day 2
Day 4
Days Post Infection
ND Sham
ND High Dose
HFD Sham
HFD High Dose

Figure 8

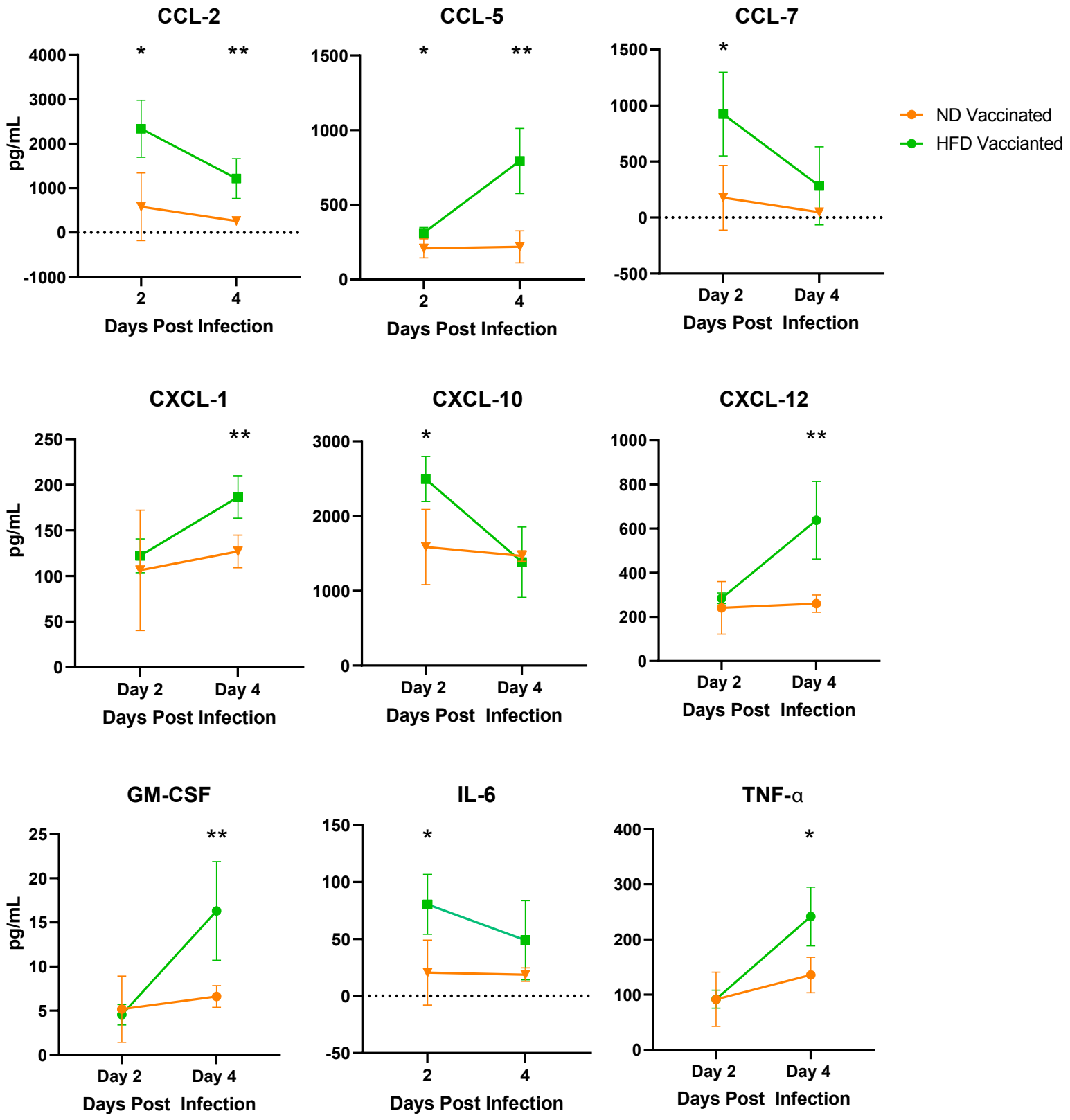
CCL-2
CCL-5
CCL-7
CXCL-1
CXCL-10
CXCL-12
GM-CSF
IL-6
TNF-α
pg/mL
Days Post Infection
Day 2
Day 4
ND Vaccinated
HFD Vaccianted